Charge relaxation rates in insulating straight capillaries

Eric Giglio

Charge relaxation rates in insulating straight capillaries

Giglio Eric
Centre de Recherche sur les Ions, les Matériaux et la Photonique (CIMAP), Normandie Univ, ENSICAEN, UNICAEN, CEA, CNRS, F-14000 Caen, France
(Dated: January 24, 2024)

The charge relaxation of accumulated charge patches in insulating straight capillaries is investigated theoretically. The model assumes that charges accumulate only at the inner and outer insulator-vacuum interface of the capillary but not in the bulk. We give an analytical solution to the coupled equations that describe the surface charge dynamics at both interfaces. We provide a tool to calculate easily the characteristic relaxation times in a straight capillary of any dimension, possibly surrounded by a conducting cylinder. The latter allows for different scenarios found in experimental setups, and is applicable to both nano and macro-capillaries. We propose an original experimental technique to monitor the charge relaxation in a straight glass capillary and show how to use the presented model to extract the bulk and surface conductivity of the insulator from the measured data. In the supplementary material, we provide a script in ®Mathematica that allows the reader to compute comfortably the decay rates for all straight insulating capillaries the reader is interested in.

PACS numbers: 34.80.Dp, 34.80.Pa

I. INTRODUCTION

When low energetic ions hit an insulating surface, charge carriers are injected at the impact points and trapped by defects. As a result, charge accumulates in the dielectric, generating an electric field that, if sufficiently strong, deviates the following beam particles, preventing them to hit the insulator surface. This basic property led to the discovery that slow ions can pass through insulator capillaries (having an aspect ratio, length over diameter, larger than 50) without any change, neither in the ion charge state nor in the ion kinetic energy, even when the geometrical conditions do not allow it. The phenomenon is called charged particle guiding by insulating capillaries and it has become an intensively studied field since its discovery by the pioniering work by N. Stoltherfoht for polyethylene terephthalate (PET) nano-capillaries [1] and T. Ikeda for glass macro-capillaries [2], more than 10 years ago.

On the experimental front, charge relaxation in insulating capillaries was recently investigated by several authors. The charge decay of a previously charged conical glass capillary was monitored by recording the deflection of a by-passing ion beam on a PSD [3]. The measured decay time of 2000 min was used to adjust the surface conductivity in simulations. Dubois *et al.* monitored the decay of charge patches in a glass tube [4]. After charging a glass tube by a tilted 1 keV Ar^+ beam, the charge patch was allowed to discharge for a given time. After that time, the beam was re-injected, and the initial transmitted fraction was given as a function of the discharge time. In Nagy *et al.*, a micrometer sized proton beam of 1 MeV, tilted by 1°, was center injected into a Teflon capillary with macroscopic dimensions [5]. With increasingly accumulated charge, the patch got sufficiently strong to deflect the beam out of the capillary on a screen downstream. A dynamical equilibrium between the charges being deposited and flowing away in form of leakage current was found. The leakage current was estimated to 10 % of the injected current.

While nowadays the guiding of ions through glass-capillaries due to charge patches is qualitatively understood, the complex nature of the electric conduction in such insulators makes quantitative theoretical predictions still a challenging task. Indeed, for a given ion beam, the guiding is entirely controlled by the dynamics of the charge patches in the dielectric, which in turn depend on the electrical properties of insulator, on the possible presence of electrodes that affect the electric field inside the capillary and on the charge transfer at the interfaces.

In the past, numerous theoretical approaches succeeded to capture the guiding properties of insulating capillaries, by using in their simulations appropriate charge relaxation times (also called decay times) for the exponential decay of the accumulated charges [6, 7]. Typically, by varying the decay times, observed trends in the guiding process of ion beam through capillaries could be reproduced numerically [8–13]. The success of those models showed that the charge dynamics in insulators is already well described by a simple exponential decay of the accumulated charge distribution. It seems thus that having an accurate relationship between the charge relaxation rate of an accumulated charge distribution and the geometrical and electrical properties of the capillary, would be beneficial for (i) making reliable theoretical predictions, by knowing the electrical properties of the capillary, or (ii) deducing the electrical properties of the capillary by measuring the decay rates. Being able to refine the computing of the relaxation rates would allow for deeper understanding of the influence of the bulk and surface conductivity and dimensions of the capillary on the charge dynamics in capillaries.

An initial guess of the decay rate was usually obtained by considering the bulk conductivity, diffusion and dielec-

tric constant of the insulating capillary. For example, in macro-capillaries, the order of magnitude of the depletion rate was estimated using the expression $2\kappa_b/[\varepsilon_0(1+\varepsilon_r)]$, with κ_b being the bulk conductivity and ε_r the dielectric constant of the insulator [8, 12, 13]. The screening factor $2/(1+\varepsilon_r)$ corresponds to the screening of a charge lying at the insulator-vacuum interface of an infinite dielectric plane. Alternatively, the more common bulk relaxation rate $\kappa_b/(\varepsilon_0\varepsilon_r)$ could be used. In nano-capillaries, the relaxation rate was estimated by Schiessl *et al.* using the surface diffusion constant [11].

Usually the surface conductivity κ_s of the insulator-vacuum interface was not directly used for estimating the decay rates, supposedly because the surface conductivity of an insulating surface is mainly due to adsorbed impurities and is thus not a well-known quantity and because the relation between the surface conductivity and the relaxation rates is not easy to establish. That does not mean that surface currents were not considered in the simulations. For nano-capillaries, the surface currents were evaluated by means of a drift model, where the accumulated charge carriers were field-driven along the surface, with a velocity proportional to their surface mobility [14, 15], and surface currents were even shown to be the dominant relaxation channel. For macroscopic glass capillaries, the surface currents were taken proportional to the insulator-vacuum surface conductivity [3]. However, for the estimation of the total charge relaxation rate, the influence of the surface conductivity κ_s was systematically ignored.

The present work models the charge dynamics in straight insulating capillaries and extracts from the equations the relaxation rates that characterize the charge dynamics. It gives the explicit dependency of the relaxation rates on the geometric dimensions and macroscopic electrical properties of the capillary. Much attention is payed to the electric field that drives the charges in the insulator, so that reliable relaxation rates can be deduced from the model. Here, the electric field is evaluated by considering the appropriated boundary conditions that describe the capillary and its environment. In other words, the electric field includes the exact contribution of induced polarization charges (image charges) that appear at the interfaces separating two dielectric media and that screen the accumulated charges in the dielectric. The contribution of the surface conductivity (at the insulator-vacuum interface) to the total charge relaxation rate is clearly established and can be estimated quantitatively with the model.

In a preliminary work, Giglio *et al.* evaluated the charge relaxation rates of a surface charge distribution at the inner surface of a straight glass capillary with the outer surface grounded [16]. The charge dynamics equation at the inner surface was solved by projecting the charge distribution onto a multipole expansion. The results showed that each multipole moment has its own relaxation rate, with the latter being the weighted sum of the bulk and surface conductivity. For each moment, the weights are different and depend only on the dimensions of the capillary. Those findings where then used to analyze the experimental results given in [4].

In this manuscript we will go a step further and treat the more general case where the outer surface of the capillary is no longer electrically grounded but simply the dielectric-vacuum interface where charges can accumulate and be injected. We add to the model a third conducting cylindrical interface that surrounds the capillary. Depending on the radius of the conducting cylindrical interface, the model can describe various setup scenarios found in the literature. The presented model can be applied to straight macroscopic glass capillaries as well as to straight nano-capillaries in membranes and thin insulating foils.

The manuscript is structured as follow. In section II, we give the the coupled differential equations that describe the charge dynamics in the capillary. We give an analytic solution of the differential equations that satisfies exactly the boundary conditions, which in turn describe the capillary and its environment. In section III, we present a Gedankenexperiment where the analytic solution is used to predict an observable as a function of the dimensions and electrical properties of a straight capillary. We show how to use the theoretical prediction to deduce the bulk and surface conductivity of the capillary from the measured observable. In the supplementary material, the author provides a script for ®Mathematica [18] that calculates the charge relaxation rates for a given capillary. The script can also evaluate the decay of the electric field in the capillary, if the initial charge distribution is given.

II. THEORETICAL MODEL

Consider a straight insulating glass capillary of length H, with R_1 and R_2 being the inner and outer radius of the capillary tube, as depicted in Fig.1. The electric properties of the capillary are given by the relative permittivity $\varepsilon_r > 1$, the bulk conductivity κ_b and surface conductivity κ_s, which we consider here all constant. The surface conductivity of an insulating surface is usually due to adsorbed impurities and expressed in Siemens (S). In the atmosphere for example, the surface conductivity of glass samples depends strongly on the humidity in the atmosphere, meaning that the adsorbed water ions are the main contributors to the anomalous large surface conductivity for glasses in the atmosphere. In near vacuum, the humidity is clearly low and the surface conductivity decreases by several orders of magnitude with respect to the humid atmosphere. It was found by Gruber *et al.* [19] that the surface conductivity in Borosilicate glass follows an Arrhenius type law, with a typical value of $\kappa_s = 10^{-16}$ S at room temperature.

We suppose that the capillary is surrounded by an electrically conducting (metal) cylinder of radius R_3 and length H, sharing the same symmetry axis than the cap-

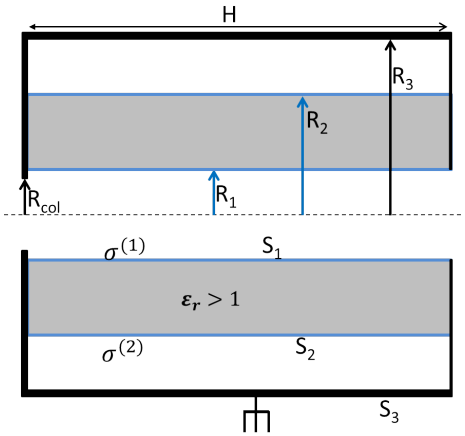

FIG. 1: Cut of the capillary along the xOz plane containing the symmetry axis. Black fat lines stand for grounded surfaces, namely the S_3 interface, the entrance and the outlet of the capillary. Grey rectangles represent the dielectric bulk. Blue lines stand for vacuum-insulator interfaces of the inner (S_1) and outer (S_2) capillary surface, carrying the surface charge densities $\sigma^{(1,2)}$.

illary. Let us label S_1 the vacuum-insulator interface of the inner capillary surface and S_2 the insulator-vacuum interface of the outer capillary surface. S_3 stands for the vacuum-conductor interface of the cylindrical surface of radius R_3. The potential V_3 of the S_3 interface may be imposed or floating. With respect to the previous model presented in [16], interface S_3 is an important addition, making the present model quite general. In particular, it allows us to impose a Dirichlet boundary condition to the electric potential, defining it uniquely. The latter suggests that in experiments, a conducting cylinder should surround the capillary if a reliable comparison between experiments and theory is desired. We study here merely the case, found in many experimental setups, where the interface S_3 is electrically grounded, $V_3 = 0$ [3, 13, 19–25] We further suppose that the capillary is mounted behind a grounded collimator plate with an inlet hole for the ion beam of radius $R_{\rm col} < R_1$, avoiding the charging-up of the entrance.

In alkali silicate glasses like borosilicate, the mobility of holes, electrons and anions is usually small compared to the mobility of alkali ions, so that the charge transport in ionic glasses at room temperature is entirely due to mobile alkali ions [26–30]. We further assume that the rate τ_h^{-1} at which the injected holes migrate into the bulk is negligible compared to the charge relaxation rate due to the bulk conductivity,

$$\tau_h^{-1} \ll \tau_b^{-1} = \frac{\kappa_b}{\varepsilon_0 \varepsilon_r} \quad . \tag{1}$$

The latter suggests that, as soon as a hole migrates from the surface into the bulk, the hole is "quickly" relaxed by the migration of alkali ions (away from the hole) so that no charge accumulates in the bulk. As a result, the charge accumulates only at the interfaces and may be represented by the surface charge densities $\sigma^{(1)}$ and $\sigma^{(2)}$ at the inner and outer interfaces respectively. The electric field that drives the alkali ions in the bulk is thus divergence-free, $\vec{\nabla} \cdot \vec{E} = 0$. Using cylindrical coordinates (r, θ, z), the dynamics of the surface charge densities $\sigma^{(1)} \equiv \sigma(R_1, \theta, z, t)$ and $\sigma^{(2)} \equiv \sigma(R_2, \theta, z, t)$ are given by two surface continuity equations, which are coupled by the electric field $\vec{E}$ that depends on the surface charges $\sigma^{(1,2)}$,

$$\frac{\partial \sigma^{(1)}}{\partial t} = -\kappa_b E_r - \frac{1}{R_1}\frac{\partial}{\partial \theta}[\kappa_s E_\theta] - \frac{\partial}{\partial z}[\kappa_s E_z] + \gamma^{(1)} \ , \tag{2}$$

$$\frac{\partial \sigma^{(2)}}{\partial t} = \kappa_b E_r - \frac{1}{R_2}\frac{\partial}{\partial \theta}[\kappa_s E_\theta] - \frac{\partial}{\partial z}[\kappa_s E_z] + \gamma^{(2)} \ , \tag{3}$$

where (2) is evaluated at $r = R_1$ and (3) at $r = R_2$. The first right hand terms in equations (2-3) are proportional to the bulk conductivity κ_b and stand for the mobile charge carriers that are field driven from the inner to the outer surface (or vice-verso) by the radial component E_r of the electric field. The second and third right hand terms account for surface currents along the $\vec{u}_z$ and $\vec{u}_\theta$ directions and are proportional to the surface conductivity κ_s. The source terms $\gamma^{(1,2)}(\theta, z, t)$ represent the deposited charge per unit time and area at the interfaces S_1 and S_2, respectively. If the capillary is well screened from stray electrons [21], no charges are injected at the outer surface and $\gamma^{(2)} = 0$. Such fully screened glass capillaries were used for example in [3] in order to measure the discharge rates of pre-charged capillaries and to put into evidence the self-organized focusing by conical glass capillaries. The source term $\gamma^{(1)}$ stands for the injected holes at the inner interface by impacting beam ions and is thus proportional to the difference between the injected current $I_{\rm in}$ and the transmitted current $I_{\rm out}(t)$, $\gamma^{(1)}(\theta, z, t) \propto (I_{\rm in} - I_{\rm out}(t))$. Note that $\gamma^{(1)}$ can also include secondary electrons generated at the impact point and absorbed elsewhere at the inner surface. The analytic solution of coupled continuity equations (2-3) is obtained using a multipole expansion technique, already used in [16].

A. Multipole expansion

We assume that the beam axis and capillary axis lie in the xOy plane so that the accumulated charge in the straight capillary has xOy plane symmetry. The interfaces S_1 and S_2 are in contact with the grounded collimator at $z = 0$ and grounded exit at $z = H$. Hence, no charges accumulate at the grounded entrance and exit so that the free surface densities are zero at $z = 0$ and $z = H$. We may then expand the surface densities $\sigma^{(1,2)}$

on the following basis which accounts for the xOy plane symmetry and zero density at the capillary entrance,

$$\sigma^{(1)}(\theta,z,t) = \sum_{m,n}\sigma^{(1)}_{mn}(t)\cos(m\theta)\sin(k_n z) \quad , \quad (4)$$

$$\sigma^{(2)}(\theta,z,t) = \sum_{m,n}\sigma^{(2)}_{mn}(t)\cos(m\theta)\sin(k_n z) \quad . \quad (5)$$

where $m \geq 0$ stands for the angular moment of the distribution. Choosing the wave number k_n of index $n \geq 1$ to be defined as

$$k_n = \frac{n\pi}{H} \quad , \quad (6)$$

ensures that the surface densities are zero at the exit of the capillary. We further assume that the grounded entrance and exit hinder charges to be injected at $z = 0$ and $z = H$, so that the injection cross-sections $\gamma^{(1)}$ and $\gamma^{(2)}$ are expanded similarly,

$$\gamma^{(1)}(\theta,z,t) = \sum_{m,n}\gamma^{(1)}_{mn}(t)\cos(m\theta)\sin(k_n z) \quad ,$$

$$\gamma^{(2)}(\theta,z,t) = \sum_{m,n}\gamma^{(2)}_{mn}(t)\cos(m\theta)\sin(k_n z) \quad .$$

The electric field being divergence-free in the bulk and outside the bulk, the electric potential V satisfies the Laplace equation everywhere, $\vec{\nabla}^2 V = 0$. We distinguish 3 regions in space, bound by the three interfaces S_1, S_2 and S_3. We further assume that the potential is zero (grounded) at the entrance $z = 0$ and exit $z = H$ of the capillary. Within the above assumptions, a general solution of the Laplace equation in cylindrical coordinates for all three regions of space is eventually given by,

$$V^{(1)}(r,\theta,z,t) = \sum_{m,n} A_{mn}(t) I_m(k_n r)\cos(m\theta)\sin(k_n z), \quad 0 \leq r \leq R_1 \quad (7)$$

$$V^{(2)}(r,\theta,z,t) = \sum_{m,n}\left[B_{mn}(t)I_m(k_n r) + C_{mn}(t)K_m(k_n r)\right] \times \cos(m\theta)\sin(k_n z) \ , \quad R_1 \leq r \leq R_2 \quad (8)$$

$$V^{(3)}(r,\theta,z,t) = \sum_{m,n}\left[D_{mn}(t)I_m(k_n r) + E_{mn}(t)K_m(k_n r)\right] \times \cos(m\theta)\sin(k_n z) \ , \quad R_2 \leq r \leq R_3 \quad (9)$$

where $I_m()$ and $K_m()$ are modified Bessel functions of order $m \geq 0$. Note that a zero potential condition at the exit of the capillary is not strictly required here, but it simplifies the mathematical expressions without loosing much of the general scope. We also note that for $r < R_{\rm col}$, the potential $V^{(1)}$ is obviously not imposed at the entrance and $V^{(1)}$ is thus not rigorously zero for $z = 0$. However, for $r < R_{\rm col}$ the potential $V^{(1)}$ at the entrance can be assumed sufficiently close to zero so that the $V^{(1)}(z = 0) = 0$ conditions can nevertheless be imposed without introducing a significant bias in the final results The five terms $A_{mn}(t), B_{mn}(t) \ldots E_{mn}(t)$ found in (7-9) are defined by the boundary and kinematic conditions given below.

B. Boundary Conditions

In order to define unambiguously the potentials in the three domains, we need to add 5 boundary conditions. The electric potential is continues at the three interfaces. Consequently, the potentials $V^{(1,2,3)}$ defined in the three domains must satisfy the boundary conditions,

$$(S_1): \quad V^{(1)}(R_1,\theta,z,t) = V^{(2)}(R_1,\theta,z,t) \quad (10)$$

$$(S_2): \quad V^{(2)}(R_2,\theta,z,t) = V^{(3)}(R_2,\theta,z,t) \quad (11)$$

$$(S_3): \quad V^{(3)}(R_3,\theta,z,t) = V_3 = 0 \quad , \quad (12)$$

with $V_3 = 0$ standing for the grounded potential of the conducting interface S_3. At the interface separating two dielectric media, the electric field normal to the interface is discontinues. In the presence of free surface charges one has,

$$(S_1): \quad -\varepsilon_r \left.\frac{\partial V^{(2)}}{\partial r}\right|_{r=R_1} + \left.\frac{\partial V^{(1)}}{\partial r}\right|_{r=R_1} = \frac{\sigma^{(1)}(t)}{\varepsilon_0} \quad (13)$$

$$(S_2): \quad -\left.\frac{\partial V^{(3)}}{\partial r}\right|_{r=R_2} + \varepsilon_r \left.\frac{\partial V^{(2)}}{\partial r}\right|_{r=R_2} = \frac{\sigma^{(2)}(t)}{\varepsilon_0} \quad (14)$$

From the above boundary conditions, we deduce that the terms $A_{mn}(t), B_{mn}(t) \ldots E_{mn}(t)$ found in (7-9) can be written as a linear combination of both time-dependent surface charge densities moments $\sigma^{(1,2)}_{mn}(t)$ in the form,

$$A_{mn}(t) = a^{(1)}_{mn}\sigma^{(1)}_{mn}(t) + a^{(2)}_{mn}\sigma^{(2)}_{mn}(t) \quad (15)$$

$$\vdots$$

$$E_{mn}(t) = e^{(1)}_{mn}\sigma^{(1)}_{mn}(t) + e^{(2)}_{mn}\sigma^{(2)}_{mn}(t) \quad (16)$$

The constant coefficients $a^{(i)}_{mn} \ldots e^{(i)}_{mn}$, $i = 1, 2$ are known quantities that depend on the parameter $R_1, R_2, H, \varepsilon_r$ of the capillary as well as on R_3. This means that the influence of the dimensions of the capillary, its dielectric constant and the dimensions of the surrounding metal cylinder are hidden in those constant coefficients. Details about how to evaluate the coefficients $a^{(i)}_{mn} \ldots e^{(i)}_{mn}$, $i = 1, 2$ are given in the Appendix A. Eventually, the expression of the electric potentials $V^{(2)}(r,\theta,z,t)$, which will be needed in the next section, reads

$$V^{(2)} = \sum_{mn}\Big[\left(b^{(1)}_{mn}I_m(k_n r) + c^{(1)}_{mn}K_m(k_n r)\right)\sigma^{(1)}_{mn}(t) + \left(b^{(2)}_{mn}I_m(k_n r) + c^{(2)}_{mn}K_m(k_n r)\right)\sigma^{(2)}_{mn}(t)\Big] \times \cos(m\theta)\sin(k_n z) \quad , \quad (17)$$

where the dependence on time is explicitly given by the time-evolution of the surface charge densities at the inner and outer capillary interfaces. Note that, as $V^{(2)}$ satisfies the required boundary conditions (10-14), it automatically includes the contributions from the induced image charges at the interfaces S_1, S_2, and S_3.

C. General Solution of the time evolution of the surface charges

The expressions of the electric field that appear in the equations (2-3) can all be deduced from the potential $V^{(2)}$ (Eq. 17), which is defined for $R_1 \leq r \leq R_2$, so that we may re-write the equations (2-3) in the form,

$$\frac{\partial \sigma^{(1)}}{\partial t} = \kappa_b \left.\frac{\partial V^{(2)}}{\partial r}\right|_{r=R_1} - \kappa_s \left(\frac{m^2}{R_1^2} + k_n^2\right) V^{(2)}\Big|_{r=R_1} + \gamma^{(1)}$$
$$\frac{\partial \sigma^{(2)}}{\partial t} = -\kappa_b \left.\frac{\partial V^{(2)}}{\partial r}\right|_{r=R_2} - \kappa_s \left(\frac{m^2}{R_2^2} + k_n^2\right) V^{(2)}\Big|_{r=R_2} + \gamma^{(2)} \quad (18)$$

Injecting the multipole expansions of $\sigma^{(1,2)}$ (4) , $\gamma^{(1,2)}$ (5) and $V^{(2)}$ (17) into (18) and projecting the latter onto the basis elements $\cos(m\theta)\sin(k_n z)$ yields for each set of indices (m,n) a linear matrix equation of the form,

$$\begin{pmatrix} \dot{\sigma}^{(1)}_{mn} \\ \\ \dot{\sigma}^{(2)}_{mn} \end{pmatrix} = - \begin{pmatrix} f^{(11)}_{mn} & f^{(12)}_{mn} \\ \\ f^{(21)}_{mn} & f^{(22)}_{mn} \end{pmatrix} \begin{pmatrix} \sigma^{(1)}_{mn} \\ \\ \sigma^{(2)}_{mn} \end{pmatrix} + \begin{pmatrix} \gamma^{(1)}_{mn} \\ \\ \gamma^{(2)}_{mn} \end{pmatrix} \quad (19)$$

where all the dependencies on the geometry and electric properties of the insulating capillary are now hidden in the time-**in**dependent coefficients

$$f^{(1j)}_{mn} = \left(-\kappa_b I'_m(k_n R_1) + \kappa_s \left(\frac{m^2}{R_1^2} + k_n^2\right) I_m(k_n R_1)\right) b^{(j)}_{mn} + \left(-\kappa_b K'_m(k_n R_1) + \kappa_s \left(\frac{m^2}{R_1^2} + k_n^2\right) K_m(k_n R_1)\right) c^{(j)}_{mn} \quad (20)$$

$$f^{(2j)}_{mn} = \left(\kappa_b I'_m(k_n R_2) + \kappa_s \left(\frac{m^2}{R_2^2} + k_n^2\right) I_m(k_n R_2)\right) b^{(j)}_{mn} + \left(\kappa_b K'_m(k_n R_2) + \kappa_s \left(\frac{m^2}{R_2^2} + k_n^2\right) K_m(k_n R_2)\right) c^{(j)}_{mn} \quad (21)$$

where the prime symbol stands for the derivative with respect to the radial component and $j = 1, 2$. Remarkably, there is no coupling between the modes in (19), neither for the angular mode m nor for the axial mode n. As a result, (19) can be solved independently for each mode (m,n). This however is the case only for straight capillary tubes. In the case of tapered capillaries, at least the axial modes n would be coupled to other axial modes n'. For convenience, a ®Mathematica script that evaluates the matrix elements $f^{(i,j)}_{mn}$ is given in appendix B.

D. Homogeneous solution

In this work we consider only the homogeneous solution of (19), that is, the solution in the absence of source terms, $\gamma^{(1,2)}_{mn}(t) = 0$. Such a solution describes the charge relaxation of a previously accumulated charge distribution in the case where no beam is further injected into the capillary. The homogeneous solution of (19) is easily found if the matrix $F_{mn} = \{f^{(ij)}_{mn}\}$ is non-defective (diagonalizable) so that

$$\left(1/\tau^{(i)}_{mn}\right)\delta_{ij} = T^{-1}_{mn} F_{mn} T_{mn} \quad (22)$$

where the characteristic relaxation rates $1/\tau^{(1)}_{mn}$ and $1/\tau^{(2)}_{mn}$ are the two eigenvalues of the matrix F_{mn} and where T_{mn} is the change of basis matrix. The relaxation rates $1/\tau^{(1)}_{mn}$ are thus functions of the dimensions (R_1, R_2, H) and electric properties $(\varepsilon_r, \kappa_s, \kappa_b)$ of the capillary as well as the radius R_3 of the grounded cylinder surrounding the capillary. Note that because the relaxation rates $1/\tau^{(1,2)}_{mn}$ are obtained by diagonalizing the F_{mn} matrices, they are in general *non-linear* functions of the bulk and surface conductivity of the capillary. In the particular case where the outer surface S_2 is grounded, the elements $f^{(21)}_{mn}$ and $f^{(22)}_{mn}$ are zero. The matrix F_{mn} has then only one non-zero eigenvalue, namely $\tau^{(1)}_{mn} = f^{(11)}_{mn}$, which is a linear functions of κ_s and κ_b . The latter finding was already discussed in [16].

A solution of the homogeneous case is eventually given by

$$\begin{pmatrix} \sigma^{(1)}_{mn}(t) \\ \\ \sigma^{(2)}_{mn}(t) \end{pmatrix} = T_{mn} \begin{pmatrix} e^{-t/\tau^{(1)}_{mn}} & 0 \\ \\ 0 & e^{-t/\tau^{(2)}_{mn}} \end{pmatrix} T^{-1}_{mn} \begin{pmatrix} \sigma^{(1)}_{mn}(0) \\ \\ \sigma^{(2)}_{mn}(0) \end{pmatrix} \quad (23)$$

where the $\sigma^{(i)}_{mn}(0)$ are the initial (previously accumulated) surface charge distributions at the interfaces S_i. Introducing the auxiliary projector P_{mn} defined by

$$P_{mn} = T_{mn} \begin{pmatrix} 1 & 0 \\ \\ 0 & 0 \end{pmatrix} T^{-1}_{mn} \quad , \quad (24)$$

and noting $\vec{\sigma}_{mn}(t) = \begin{pmatrix} \sigma^{(1)}_{mn}(t) \\ \sigma^{(2)}_{mn}(t) \end{pmatrix}$, one can express the solution (23) in the following compact form

$$\vec{\sigma}_{mn}(t) = \left(e^{-t/\tau^{(1)}_{mn}} P_{mn} + e^{-t/\tau^{(2)}_{mn}} (I - P_{mn})\right) \cdot \vec{\sigma}_{mn}(0) \quad , \quad (25)$$

where I is the identity matrix. Equation (25) yields that, in the absence of source terms, each moment $\vec{\sigma}_{mn}(t)$ relaxes exponentially in time with two time constants $\tau^{(1)}_{mn}$

and $\tau^{(2)}_{mn}$. Eventually injecting (25) into the multipole expansion (4) and (5) gives the explicit time evolution of the surface charge densities $\sigma^{(1,2)}(\theta, z, t)$ that satisfy the surface charge equations (2) and (3) without source terms. Similarly, injecting (25) into (17) yields the electric potential that drives the charge carriers in the insulator bulk. Finally, injecting (25) into (A14) yields the electric potential inside the capillary that guides the ion beam.

E. Stationary source terms

Consider the case where the source term $\vec{\gamma}_{mn}(t) = \begin{pmatrix} \gamma^{(1)}_{mn}(t) \\ \gamma^{(2)}_{mn}(t) \end{pmatrix}$ is time independent, so that $\partial_t \vec{\gamma}_{mn}(t) = 0$ for all m, n. Such a situation may correspond to a stationary beam that injects charge at constant rate at the inner surface of a (tilted) capillary. We further assume that the capillary is initially electrically neutral, $\vec{\sigma}_{mn}(0) = 0$. The time evolution of the surface charge distributions is then given by

$$\begin{aligned} \vec{\sigma}_{mn}(t) &= \left(1 - e^{-t/\tau^{(1)}_{mn}}\right) \tau^{(1)}_{mn} P_{mn} \vec{\gamma}_{mn} \\ &+ \left(1 - e^{-t/\tau^{(2)}_{mn}}\right) \tau^{(2)}_{mn} (I - P_{mn}) \cdot \vec{\gamma}_{mn} \quad . \quad (26) \end{aligned}$$

Relationship (26) is handy if one wants to estimate the charge distribution of a patch in the capillary after a given charging time t. The relationship holds in the case of a constant or slowly (adiabatically) evolving source term.

III. DEFLECTION OF THE BEAM BY A CHARGE PATCH

The above model is quite general and useful to determine the charge relaxation rates in many different scenarios, and is not limited to macroscopic glass-capillaries. For instance the model can also be applied to nano-capillaries in insulating foils. The inner radius R_1, length H, dielectric constant ε_r and bulk conductivity κ_b of the nano-capillaries are usually given. Caution must be paid to the choice of R_2 and R_3 for the model to represent reliably the nano-capillaries in question as they are not so clearly defined as in glass macro-capillaries. We give here two examples. For nano-capillaries in PET foils, like the one used in [1], we suggest to set the radius R_2 to half of the inter-capillary distance, which in [1] was about $R_2 \simeq 2.5$ µm. As no grounded S_3 interface surrounds the nano-capillaries in PET foils, R_3 should be set to an arbitrary large value so that $R_3 \gg R_2$. The nano-capillaries in n-doped silicon membrane found in [24], have an insulating SiO_2 thickness of 100 nm. The radius R_2 may then be set to $R_2 = R_1 + 100$ nm. Because the n-doped silicon is a semi-conducting media, we can assume that the potential of the silicon media in between the nano-capillaries is grounded so that $R_3 = R_2$. The remaining unknown in both examples is then the surface conductivity. A detailed study of the charge relaxation in nano-capillaries and the analyses of the experimental data with this model will be presented elsewhere. In the present work, we will merely focus on straight glass capillaries and show how to use the model to estimate the surface and bulk conductivity of a given insulating glass capillary that was previously charged by an ion beam.

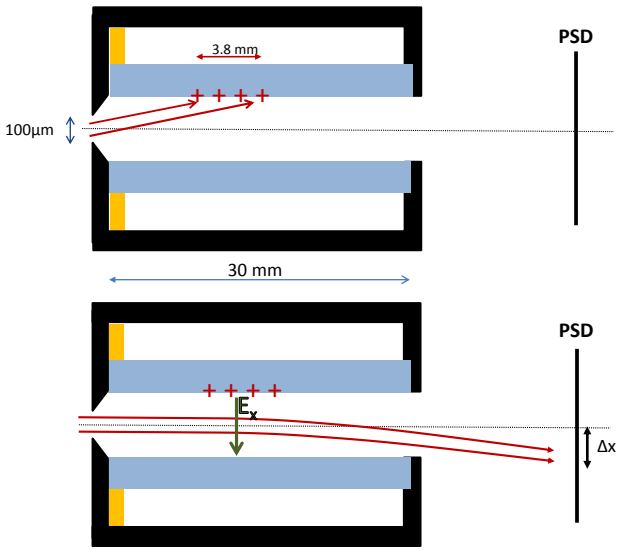

FIG. 2: Scheme of the experimental technique to monitor the relaxation of a previously injected charge patch in the case (a) where the outer surface of the capillary is **not** grounded. Glass bulk is represented by glue-gray rectangles and is surrounded by grounded layer (black full lines). The yellow parts stand for insulator rings keeping the glass tube in place. Upper panel: a tilted beam injects a charge patch at the inner surface. Lower panel: transmitted beam is deflected by the charge patch and its position $\Delta x(t)$ is recorded on the PSD located downstream.

A. Modeling a Gedankenexperiment

In the previous section, we saw how to calculate the relaxation rates, knowing the bulk and surface conductivity for a given capillary. In the following Gedankenexperiment, we will show how to estimate the bulk and surface conductivity of the capillary unambiguously, by monitoring the charge relaxation rate of a previously injected charge patch.

We consider here a straight glass capillary, with the dimensions $H = 30$ mm , $R_1 = 0.43$ mm, $R_2 = 0.75$ mm. The capillary is made out of Borosilicate glass, characterized by a dielectric constant $\varepsilon_r = 4.6$. Glass tubes like the one supposed in this Gedankenexperiment are

commercially available, for example, by Warner Instruments. We consider two different configurations. In the first configuration, labeled (a), the conducting interface S_3 has a much larger inner radius than the outer surface of the capillary, $R_2 \ll R_3 = 5$ mm. In the second configuration, labeled (b), the outer surface is grounded, $R_3 = R_2$. Both configurations are easily set up in a dedicated experiment like the one presented in [3]. The idea is to use the different charge relaxation rates that yield case (a) and (b) in order to estimate the surface and bulk conductivity of the capillary.

The experimental methodology is the following. In a first step, the axis of the capillary is tilted by 1.5° with respect to the beam axis. A charge patch, centered at $\theta = 0, z_c = R_1/\tan(1.5°) \simeq 16$ mm, is injected at the inner surface by a uniform ion beam collimated to a diameter of $b = 0.1$ mm. The intensity $I_{\rm in}$ of the injected current must be adjusted so as to produce a single patch which is strong enough to deflect a part of the injected beam through the capillary outlet. The charge patch has a characteristic length of $d = b/\tan(1.5°) \simeq 3.8$ mm in the z-direction, see upper panel of Fig.2. As soon as the charge patch is sufficiently strong to deflect a part of the beam thought the capillary outlet, the injected intensity is reduced to several fA. Reducing the beam intensity is important in order to avoid that the charge patch is neutralized by secondary electrons generated by beam ions hitting the border of the collimator hole at the entrance. At the same time, the capillary axis is aligned with the beam axis (zero tilt angle). The previously accumulated charge patch deflects now the injected beam ions of charge q and momentum $p_z\vec{u}_z$ by an angle α, which can be monitored on a position sensitive detector (PSD) downstream, see lower panel of Fig.2. In a second step, the time evolution of the deflection angle $\alpha(t)$ of the transmitted beam is recorded. The methodology is repeated for setup (a) and (b).

We will now model the time evolution of the measured deflection angle of the Gedankenexperiment and give an analytic expression of the deflection angle $\alpha(t)$ using the findings of section II. The x-component of the electric field evaluated at the symmetry axis is given by

$$\begin{aligned} E_x(0,0,z,t) &= -\left.\frac{\partial V^{(1)}(r,\theta=0,z,t)}{\partial r}\right|_{r=0} \\ &= -\sum_{n=1}\frac{n\pi}{2H}\left(\underbrace{a_{1n}^{(1)}\sigma_{1n}^{(1)}(t)+a_{1n}^{(2)}\sigma_{1n}^{(2)}(t)}_{\vec{a}_{mn}\cdot\vec{\sigma}_{mn}(t)}\right) \\ &\quad\times\sin(k_n z) \end{aligned} \tag{27}$$

with the constant coefficients $a_{1,n}^{(1)}$ and $a_{1,n}^{(2)}$ being defined in the Appendix A. Note that only dipole angular moments, $m = 1$, give a non-zero contribution to the electric field evaluated at the symmetry axis. Injecting (25) into (27) allows expressing the time-evolution of $E_x(0,0,z,t)$,

$$\begin{aligned} E_x(0,0,z,t) = -\sum_{n=1}\frac{n\pi}{2H}\Bigg[& e^{-t/\tau_{1n}^{(1)}}\underbrace{\vec{a}_{1n}\cdot P_{1n}\cdot\vec{\sigma}_{1n}(0)}_{g_n^{(1)}} \\ & + e^{-t/\tau_{1n}^{(2)}}\underbrace{\vec{a}_{1n}\cdot(I-P_{1n})\cdot\vec{\sigma}_{1n}(0)}_{g_n^{(2)}}\Bigg] \\ & \times\sin(k_n z) \quad . \end{aligned} \tag{28}$$

The scalars $g_n^{(1)}$ and $g_n^{(2)}$ give the amplitudes of the two exponential decay functions for each n and depend explicitly on the initial charge distributions $\vec{\sigma}_{1n}(0)$ at the inner and outer surface of the capillary.

In the next step, the capillary axis is aligned with the beam axis (zero tilt angle). The injected intensity is reduced to several fA, in order to avoid that the charge patch is neutralized by secondary electrons generated by beam ions hitting the border of the collimator hole at the entrance. The charge patch deflects now the beam ions of charge q and momentum $p_z\vec{u}_z$ by an angle α, which can be monitored on a position sensitive detector (PSD) downstream, see lower panel of Fig.2. The time evolution of the deflection angle $\alpha(t)$ is given by

$$\begin{aligned} \tan(\alpha(t)) &= \frac{p_x(t)}{p_z} = \frac{q}{2E_k}\int_0^H E_x(0,0,z,t)dz \\ &= \frac{1}{2V_s}\sum_{n=1,\rm odd}\left[e^{-t/\tau_{1n}^{(1)}}g_n^{(1)}+e^{-t/\tau_{1n}^{(2)}}g_n^{(2)}\right] \end{aligned} \tag{29}$$

where $E_k = qV_s$ is the kinetic energy of the ion beam. The constant amplitudes $g_n^{(1)}$ and $g_n^{(2)}$ can be evaluated if the initial surface charge moments $\vec{\sigma}_{1,n}(0)$ are known.

B. Numerical application

Borosilicate glass has typically a bulk conductivity of $\kappa_b = 10^{-13}$ S/m at room temperature, which yields a bulk relaxation time of,

$$\tau_b = \frac{\varepsilon_r\varepsilon_r}{\kappa_b} \simeq 400\,\mathrm{s} \quad . \tag{30}$$

We will later compare this value to the decay times obtained for $\alpha(t)$ in configurations (a) and (b). We further suppose a surface conductivity of $\kappa_s = 10^{-16}$ S, close to the value measured by [19] at room temperature. Both κ_b and κ_s may be regarded as initial guesses.

In order to evaluate $\alpha(t)$ numerically, using (29), we need to provide a spatial profile of the accumulated charge distribution at the interfaces after the initial charging step. To avoid unnecessary complexity, we assume that a single patch has been injected in the capillary. Note that the time evolution of the deflection angle $\alpha(t)$ in not very sensitive to the exact profile of the

	$R_3 \gg R_2$ (a)				$R_3 = R_2$ (b)			
n	$\tau_{1,n}^{(1)}$ (s)	$\tau_{1,n}^{(2)}$ (s)	$g_n^{(1)}$ (V)	$g_n^{(2)}$ (V)	$\tau_n^{(1)}$ (s)	$\tau_{1,n}^{(2)}$ (s)	$g_n^{(1)}$ (V)	$g_n^{(2)}$ (V)
1	94	295	83.5	4.5	204	$\geq 10^4$	35.4	0
3	94	293	-53.9	-3.0	204	”	-23.4	”
5	94	287	22.1	1.4	201	”	11.9	”
7	93	280	-5.6	-0.4	197	”	-3.9	”
9	92	270	0.6	0.	192	”	0.3	”
$G_1(V)$			48				19.7	

TABLE I: Characteristic times $\tau_{1,n}$ and amplitudes g_n for $m = 1$ and $n < 10$. Left part of the table gives the values for setup (a) and right part of the table for setup (b). For $n \geq 10$, the amplitudes g_n are negligible and thus omitted. Last line gives the total amplitude $G_1 = \sum_n g_n^{(1)}$.

injected charge patch as the profile controls mainly the initial amplitude of the deflection angle. For the sake simplicity, we assume that the charge patch at the interface S_1 has a Gaussian profile of the form

$$\sigma^{(1)}(\theta, z, t = 0) = \frac{Q}{b\pi d} \exp\left(-\frac{(z - z_c)^2}{d^2}\right) \exp\left(-\frac{(R_1\theta)^2}{b^2}\right) , \tag{31}$$

where $Q = 50$ pC is the total charge of the patch. The value of Q will be justified later. The lengths d and b are related to the beam size and tilt angle and were already defined in section III A. The Gaussian profile is already a good approximation of the charge distribution generated by the thin ion beam at the inner surface of the capillary, as we could check with our simulations. At the interface S_2, the charge distribution is assumed zero, $\sigma_2(\theta, z, 0) = 0$.

In a first step, we take the multipole expansion (4) of the surface charge density $\sigma^{(1)}(\theta, z, t = 0)$. We retain only the dipole angular moments $\sigma_{1,n}^{(1)}(0)$, which enter Eq. 28 . The Gaussian charge patch has a typical length along the Oz axis of $d = 3.8$ mm and is thus already well approached by an expansion limited to the first $n \leq N = (H/d) + 1 \simeq 9$ modes. In a second step, we evaluate for both cases (a) and (b), the characteristic times $1/\tau_{1,n}^{(1,2)}$, for all $n \leq N$ using, for example, the Mathematica script found in the supplementary material and described in Appendix B. In a third step, we calculate for both setups the amplitudes $g_n^{(1)}$ and $g_n^{(2)}$ defined in (28). An option in the provided Mathematica script allows computing all the required amplitudes.

In table I we give, for the first $n \leq 9$ the rates $1/\tau_{1,n}^{(1,2)}$ and amplitudes the $g_n^{(1,2)}$ that contribute to the deflection angle in (29). First we note that for case (a), $g_n^{(2)}$ is systematically one order of magnitude smaller than $g_n^{(1)}$. For case (b), the terms $g_n^{(2)}$ are zero. For both cases, we neglect thus the contributions of $g_n^{(2)}$ to the deflection angle α. Second, we note that for both configurations (a) and (b), the rates $1/\tau_{1,n}^{(1)}$ vary by less than 10% over the range $n \in [1, 9]$. We may thus approach $\tau_{1,n}^{(1)} \simeq \tau_{1,1}^{(1)}$, $\forall n \leq N$, so that the expression of the deflection angle (29) simplifies, for both cases (a) and (b), to

$$\tan(\alpha(t)) \simeq \frac{1}{2V_s} e^{-t/\tau_{1,1}^{(1)}} \underbrace{\sum_{n=1,\text{odd}}^{N} g_n^{(1)}}_{G_1} \tag{32}$$

$$= \frac{1}{2V_s} G_1 e^{-t/\tau_{1,1}^{(1)}} \tag{33}$$

The model eventually predicts that the deflection amplitude $\alpha(t)$ of the transmitted beam decays exponentially in time with a decay time equal to the relaxation time $\tau_{1,1}^{(1)}$ obtained by diagonalizing the matrix $F_{1,1}$, see (22) The constant G_1 has the dimension of an electric potential and controls the amplitude of the deflection angle α. In the last line of table I, we give G_1 for both configurations (a) and (b). Assuming for the extraction potential V_s of the ion source a value of $V_s = 1.5$ kV, we get for the case (a) the time evolution of the deflection angle, which in the small angle approximation reads (in radians),

$$\alpha(t) \simeq \frac{1}{60} \exp(-t/94) \qquad R_3 \gg R_2 \quad . \tag{34}$$

In setup (b) where the outer surface of the capillary is grounded, the deflection amplitude is reduced by more than a factor 2 and evolves with a time constant of 133 s, about three times larger than for case (a),

$$\alpha(t) \simeq \frac{1}{150} \exp(-t/204) \quad . \quad R_3 = R_2 \quad . \tag{35}$$

Comparing the decay times of setup (a), 94 s and (b), 204 s to the significantly larger bulk relaxation time $\tau_b = 400$ s, highlights the non-negligible influence of the surface conductivity on the decay rates, in the case where $\kappa_s = 10^{-16}$ S and $\kappa_b = 10^{-13}$ S/m. We note that it is important not to overcharge the patch. In configuration (a), a total charge patch of $Q = 50$ pC yields a deflection amplitude of 1/60 rad, which is sufficiently low so that the deflected beam will not hit the opposite capillary wall before exiting the capillary, while the deflection is sufficiently large to be measured on a PSD some 300 mm downstream.

C. Deducing κ_b and κ_s from the decay measurements of setups (a) and(b)

In the previous section, we showed that the model can predict the decay rate of the deviation angle $\alpha(t)$, knowing the bulk and surface conductivities of a glass tube. In Fig.3, we give the dependency of $1/\tau_{1,1}^{(1)}$ as a function of κ_s for two different bulk conductivities, namely $\kappa_b = 10^{-13}$ S/m and $\kappa_b = 5 \times 10^{-13}$ S/m and for both configurations (a) and (b). For setup (b), the decay rate $1/\tau_{1,1}^{(1)}$ depends linearly on both surface and bulk conductivity, as can

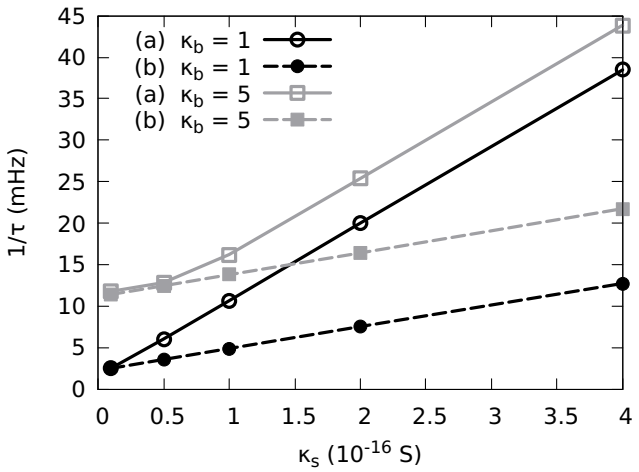

FIG. 3: Decay rate $1/\tau^{(1)}_{1,1}$ as a function of the surface conductivity κ_s for both configurations (a) and (b). Full and empty circles are obtained using a bulk conductivity $\kappa_b = 10^{-13}$ S/m; full and empty squares were calculated using $\kappa_b = 5 \times 10^{-13}$ S/m.

be deduced from the curves with filled circles and filled squares. The linear relationship was already pointed out in [16]. For setup (a) however, the relation is nonlinear as is shown by the curve with the empty squares close to the origin. This is not surprising as the rates are the zeros of the characteristic polynomial of order two of the matrix F_{mn}, see (22).

In this paragraph we want to show how to deduce the bulk and surface conductivity from the decay measurements. As we have two unknowns, (κ_b, κ_s), we need two independent measurements of $1/\tau^{(1)}_{1,1}$. The latter requirement is fulfilled by configurations (a) and (b) as can be seen by the different slopes they yield in Fig.3. Monitoring the decay of the deflection angle $\alpha(t)$ of the transmitted beam on a PSD and then fitting its time-evolution using expression (33) allows to deduce the experimental relaxation rate $\tau^{(1)}_{1,1}$ of the dipole angular moment of the charge distribution. The rates measured in case (a) and (b) should permit us to uniquely estimate the surface conductivity κ_s and bulk conductivity κ_b of the glass tube.

In the particular case where the measured decay rates of both configurations are the same, the model predicts that the charge relaxation rate is dominated by the bulk conductivity and the surface conductivity may be neglected in the model (2,3). On the contrary, if the measured rates (a) and (b) differ sensibly, then the surface conductivity has a non-negligible influence on the charge dynamics. In the latter case, using the provided Mathematica script and a Newton type search technique, a pair of (κ_b, κ_s) that yields the measured $1/\tau^{(1)}_{1,1}$ for case (a) and (b) should eventually be found. If no such pair of bulk and surface conductivities can be found, that would involve that the model does not describe realistically the the charge dynamics in the capillary. The experiment should thus provide a stringent test for the model.

IV. CONCLUSION

We proposed a simple model that describes the charge dynamics in straight insulating capillaries. The model is based on the assumption that the charges accumulate only at the inner and outer interface of the capillary. The current density through the bulk is proportional to the bulk conductivity. The surface currents along the interface are proportional to the surface conductivity. Within theses assumptions, the model is solved using a multipole expansion of the electric potential that satisfies the given boundary conditions. The model predicts the time evolution of the accumulated surface charge distribution in the presence of electrons and holes injected at the inner and outer surface. The model is applicable to a large number of systems, including nano-capillaries. It yields the charge relaxation rates that characterize the dynamics of charge patches as a function of the geometric dimensions and electric properties of the capillary. In the case of time independent source terms, it also allows to calculate the surface charge distributions that accumulate at the interfaces obtained after a given charging time.

We present a Gedankenexperiment that measures the relaxation rates of the dipole part of the accumulated charge at the capillary interfaces. We showed how to use the model in order to extract from the measurements the surface and bulk conductivity of the capillary. Upcoming experimental measurements, based on the proposed Gedankenexperiment should clarify if the surface conductivity can be omitted in the simulations and if the surface charge approximation is applicable in glass capillaries. Preliminary experimental work has already started.

For the readers interested in developing numerical codes for the charge transport through insulating capillaries, the model proposes a CPU efficient technique for the evaluation of the electric field, knowing the charge distribution at the capillary interfaces. We provide a script in ®Mathematica that calculates the quantities presented in the manuscript and which may be easily modified to calculate those quantities for various setups the reader imagines. Finally, the present model may be easily extended to account also for tapered capillaries. Work in this direction is underway.

Appendix A: Expression of the potential as a function of the surface charge densities

This appendix details the evaluation of the time independent coefficient $a^{(i)}_{mn}$, $b^{(i)}_{mn}$ and $c^{(i)}_{mn}$, $i = 1, 2$ which are needed in order to express the potentials $V^{(1)}$ and $V^{(2)}$ as functions of the surface charge densities $\sigma^{(1)}$ and $\sigma^{(2)}$. In the following, we drop the indexes m and n in the

Bessel functions in order to simplify the notations,

$$I_m(k_n R_i) \equiv I_i \quad \text{(A1)}$$
$$K_m(k_n R_i) \equiv K_i \quad \text{(A2)}$$
$$\frac{\partial}{\partial r} I_m(k_n r)\Big|_{r=R_i} \equiv I_i' \quad \text{(A3)}$$
$$\frac{\partial}{\partial r} K_m(k_n r)\Big|_{r=R_i} \equiv K_i' \quad , \quad \text{(A4)}$$

From the boundary conditions (10-14) we deduce the relations

$$A_{mn}(t) I_1 = B_{mn}(t) I_1 + C_{mn}(t) K_1 \quad \text{(A5)}$$
$$B_{mn}(t) I_2 + C_{mn}(t) K_2 = D_{mn} I_2 + E_{mn}(t) K_2 \quad \text{(A6)}$$
$$D_{mn}(t) I_3 + E_{mn}(t) K_3 = 0 \quad \text{(A7)}$$

and

$$-\varepsilon_r \left[B_{mn}(t) I_1' + C_{mn}(t) K_1'\right] + A_{mn}(t) I_1' = \frac{\sigma_{mn}^{(1)}(t)}{\varepsilon_0} \quad \text{(A8)}$$
$$-\left[D_{mn} I_2' + E_{mn} K_2'\right] + \varepsilon_r \left[B_{mn} I_2' + C_{mn} K_2'\right] = \frac{\sigma_{mn}^{(2)}(t)}{\varepsilon_0} \quad \text{(A9)}$$

The above system of equations (A5 - A9) has 5 unknowns $A_{mn}, B_{mn}, \ldots, E_{mn}$ and 5 independent linear equations, so that the unknowns are uniquely determined. It is convenient to put the above system of equations into a matrix form,

$$\begin{pmatrix} I_1 & -I_1 & -K_1 & 0 & 0 \\ 0 & I_2 & K_2 & -I_2 & -K_2 \\ 0 & 0 & 0 & I_3 & K_3 \\ I_1' & -\varepsilon_r I_1' & -\varepsilon_r K_1' & 0 & 0 \\ 0 & \varepsilon_r I_2' & \varepsilon_r K_2' & -I_2' & -K_2' \end{pmatrix} \begin{pmatrix} A_{mn} \\ B_{mn} \\ C_{mn} \\ D_{mn} \\ E_{mn} \end{pmatrix} = \begin{pmatrix} 0 \\ 0 \\ 0 \\ \sigma_{mn}^{(1)}/\varepsilon_0 \\ \sigma_{mn}^{(2)}/\varepsilon_0 \end{pmatrix} \quad \text{(A10)}$$

Solving the system of equations (A10) by a matrix inversion technique may be achieved comfortably using a technical computation software, like ®Mathematica. We remind the reader that the matrix elements depend on the indexes m, n, even if not explicitly stated. All the dependency on the dimensions (R_1, R_2, R_3, H) of the straight capillary and surrounding electrode as well as the dielectric constant ε_r of the insulator is captured by the matrix elements. The latter are thus time-independent and can be evaluated once for all for each mode (m, n). We will need in this work the explicit dependence of the electric potentials $V^{(2)}(t)$ on both time-dependent surface charge densities $\sigma_{mn}^{(1,2)}(t)$. From the structure of (A10), we deduce that the terms $A_{mn}(t)$, $B_{mn}(t)$ and $C_{mn}(t)$ can be written as a linear combination of both surface charge densities $\sigma_{mn}^{(1)}(t)$ and $\sigma_{mn}^{(2)}(t)$, namely,

$$A_{mn}(t) = a_{mn}^{(1)} \sigma_{mn}^{(1)}(t) + a_{mn}^{(2)} \sigma_{mn}^{(2)}(t) \quad \text{(A11)}$$
$$B_{mn}(t) = b_{mn}^{(1)} \sigma_{mn}^{(1)}(t) + b_{mn}^{(2)} \sigma_{mn}^{(2)}(t) \quad \text{(A12)}$$
$$C_{mn}(t) = c_{mn}^{(1)} \sigma_{mn}^{(1)}(t) + c_{mn}^{(2)} \sigma_{mn}^{(2)}(t) \quad \text{(A13)}$$

where the constant coefficients $a_{mn}^{(i)}$, $b_{mn}^{(i)}$ and $c_{mn}^{(i)}$, $i = 1, 2$ are known quantities obtained by inverting the matrix (A10) for each set of indexes (m, n). Eventually the potential $V^{(1)}(r, \theta, z, t)$ and $V^{(2)}(r, \theta, z, t)$ are expressed using explicitly the surface charge densities,

$$V^{(1)} = \sum_{mn} I_m(k_n r) \left[a_{mn}^{(1)} \sigma_{mn}^{(1)}(t) + a_{mn}^{(2)} \sigma_{mn}^{(2)}(t)\right] \times \cos(m\theta) \sin(k_n z) \quad \text{(A14)}$$

and

$$V^{(2)} = \sum_{mn} \Big[\left(b_{mn}^{(1)} I_m(k_n r) + c_{mn}^{(1)} K_m(k_n r)\right) \sigma_{mn}^{(1)}(t) + \left(b_{mn}^{(2)} I_m(k_n r) + c_{mn}^{(2)} K_m(k_n r)\right) \sigma_{mn}^{(2)}(t)\Big] \times \cos(m\theta) \sin(k_n z) \quad \text{(A15)}$$

The potential $V^{(3)}(r, \theta, z, t)$ can be obtained similarly.

Appendix B: Script for evaluating numerically the characteristic times $\tau_{mn}^{(i)}$

We provide a script for ®Mathematica 5 or above that calculates the characteristic times $\tau_{mn}^{(1)}$ and $\tau_{mn}^{(2)}$ for all $m \in [0, M_{\max}]$ and $n \in [1, N_{max}]$. The script named "rates.nb" takes as input the dimensions R_1, R_2, H, dielectric constant ε_r and conductivities κ_b and κ_s of the straight capillary as well as the radius R_3 of the conducting interface S_3. If there is no conducting S_3 interface, R_3 can be set to an arbitrary large value, typically $R_3 \gg H$. Lengths are given in mm, surface conductivity in Siemens (S) and bulk conductivity is S/m. Finally, the routine needs the highest angular $M_{\max}$ and axial $N_{\max}$ mode for which it should perform the calculations. It outputs the matrix elements $f_{mn}^{(ij)}$ (20-21) and associated characteristic times $\tau_{mn}^{(i)}$ for the requested modes (m, n). It also includes the time independent coefficients $a_{mn}^{(i)}$, $b_{mn}^{(i)}$ $\ldots e_{mn}^{(i)}$, $i = 1, 2$, necessary to express the potential $V^{(1)}$ and $V^{(2)}$ in the form (A14) and (A15) respectively. The script is available as a separate file in the supplementary material.

Acknowledgments

This work was supported by the french research agency CNRS via the project PICS N° 245358 Hongrie 2018.

[1] N. Stolterfoht, J.-H. Bremer, V. Hoffmann, R. Hellhammer, D. Fink, A. Petrov, and B. Sulik, Phys. Rev. Lett. **88** , 133201 (2002).
[2] T. Ikeda, Y. Kanai, T. M. Kojima, Y. Iwai, T. Kambara, and Y Yamazaki, M. Hoshino, T. Nebiki and T. Narusawa, Appl. Phys. Lett. **89** , 163502 (2006).
[3] E. Giglio, S. Guillous, A. Cassimi, Phys. Rev. A **98**, 052704 (2018).
[4] R. D. DuBois, K. Tőkési, E. Giglio, Phys. Rev. A **99**, 062704, (2019).
[5] G.U.L. Nagy, E. Giglio, I. Rajta K. Tőkési , Nuc. Instrum. Methods Phys. Res., Sect. B, **460** p 216 (2019)
[6] C. Lemell, J. Burgdörfer, F. Aumayr, Progress in Surface Science, **88**, 237 (2013)
[7] N. Stolterfoht and Y. Yamazaki, Physics Reports **629**, 1-107 (2016)
[8] N. Stolterfoht, Phys. Rev. A **89**, 062706 (2014)
[9] N. Stolterfoht, Nuc. Instrum. Methods Phys. Res., Sect. B **354** 51 (2015)
[10] K. Schiessl, W. Palfinger, K. Tőkési, H. Nowotny, C. Lemell, and J. Burgdörfer, Phys. Rev. A. **72**, 062902 (2005).
[11] K. Schiessl, W. Palfinger, K. Tőkési, H. Nowotny, C. Lemell, and J. Burgdörfer, Nuc. Instrum. Methods Phys. Res., Sect. B, **258**, 150 (2007)
[12] T. Schweigler, C. Lemell, J. Burgdörfer, Nuc. Instrum. Methods Phys. Res., Sect. B, **269** , 1253 (2011)
[13] N. Stolterfoht, E. Gruber, P. Allinger, S. Wampl, Y. Wang, M. J. Simon, and F. Aumayr, Phys. Rev. A **91**, 032705 (2015).
[14] N. Stolterfoht, Phys. Rev. A **87** , 012902 (2013).
[15] N. Stolterfoht, Phys. Rev. A **87** , 032901 (2013).
[16] E. Giglio, K. Tőkési, R D DuBois, Nuc. Instrum. Methods Phys. Res., Sect. B, **460** , 234 (2019).
[17] supp mat.
[18] Wolfram Research, Inc., Mathematica, Version 5.1, Champaign, IL (2004).
[19] E. Gruber, G. Kowarik, F. Ladinig, J. P. Waclawek, D. Schrempf, F. Aumayr, R. J. Bereczky, K. Tőkési, P. Gunacker, T. Schweigler, C. Lemell and J. Burgdörfer, Phys. Rev. A **86** , 062901 (2012).
[20] E. Giglio, R.D. Dubois, A. Cassimi, K. Tőkési, Nuc. Instrum. Methods Phys. Res., Sect. B, **354**, 82 (2015).
[21] E. Giglio, S. Guillous, A. Cassimi, H. Q. Zhang, G. U. L. Nagy, and K. Tőkési, Phys. Rev. A **95**, 030702(R) (2017).
[22] E. Giglio , R. D. DuBois , and K. Tőkési Nuc. Instrum. Methods Phys. Res., Sect. B, Journal of Physics: Conference Series **635** , 042010 (2015).
[23] E. Gruber, N. Stolterfoht, P. Allinger, S. Wampl, Y. Wang, M. J. Simon, F. Aumayr, Nuc. Instrum. Methods Phys. Res., Sect. B, **340**, 1-4 (2014).
[24] H.-Q. Zhang, P. Skog, and R. Schuch, Phys. Rev. A **82**, 052901 (2010).
[25] Víkor, Gy., Kumar, R. T. Rajendra, Pešic. D., Stolterfoht, N., Schuch, R., Nuc. Instrum. Methods Phys. Res., Sect. B, **233**, 218 (2005).
[26] J.J.Muray, J. Appl. Phys. **33** , 1517 (1962).
[27] D. Ravaine, J.L. Souquet. Physics and chemistry of glasses **18** , 27 (1977).
[28] D. Ravaine, J.L. Souquet. Physics and chemistry of glasses **19** , 115 (1977).
[29] Souquet JL, Nascimento ML, Rodrigues AC. J. Chem. Phys. **132**, 034704 (2010).
[30] M. Neyret, M. Lenoir, A. Grandjean, N. Massoni, B. Penelon, M. Malki, Journal of Non-Crystalline Solids, **410**, 74-81 (2015).
Phys. Rev. A **79** , 012711 (2009).